Supporting Information

Elastic Photonic Microbeads as Building Blocks for Mechanochromic Materials

Gun Ho Lee[†], Sang Hoon Han[†], Jong Bin Kim[†], Dong Jae Kim[†], Sangmin Lee[†], Wahyu Martumpal Hamonangan[†], Jung Min Lee[‡], and Shin-Hyun Kim[†,*]

[†] Department of Chemical and Biomolecular Engineering, KAIST, Daejeon 34141, South Korea

[‡] The 4th R&D Institute, Agency for Defense Development, Daejeon 34060, Republic of Korea

* To whom correspondence should be addressed. Email: kim.sh@kaist.ac.kr

S1. Characterization of polydopamine nanoparticles

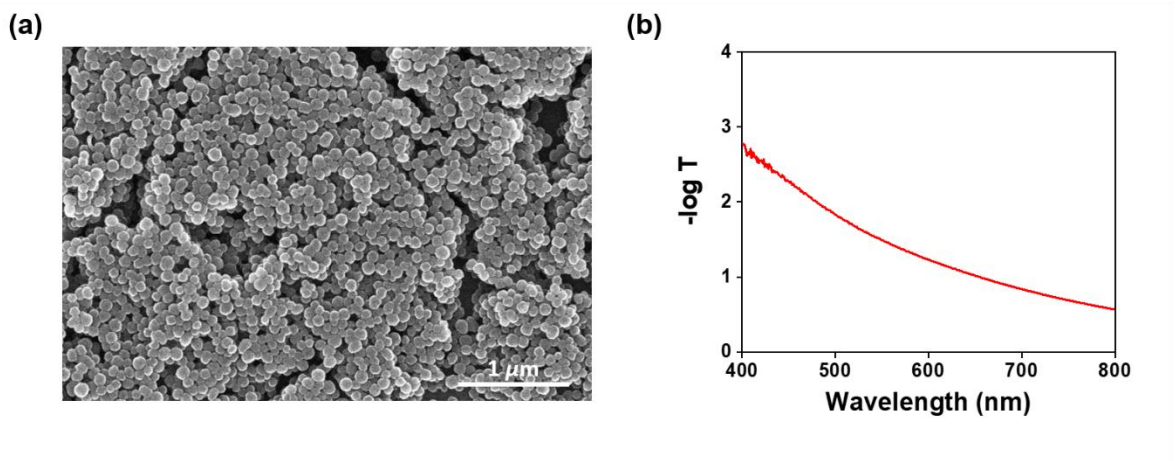

Figure S1. (a) SEM image of polydopamine nanoparticles synthesized by oxidative polymerization of dopamine precursors. (b) The extinction spectrum of polydopamine nanoparticles with the concentration of 0.278 w/w% dispersed in PEGPEA, where the thickness of dispersion is 0.4 cm.

S2. The size distribution of microbeads

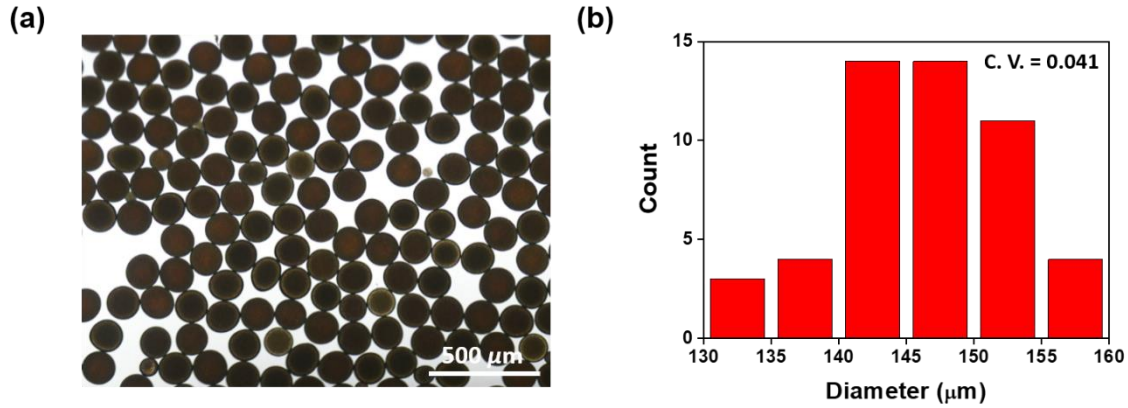

Figure S2. (a) OM image of elastic microbeads taken at transmission mode. (b) The size distribution of elastic microbeads. The average diameter is 146 μm and its coefficient of variation (C. V.) is 0.041.

S3. Diameter dependence of resonant wavelength

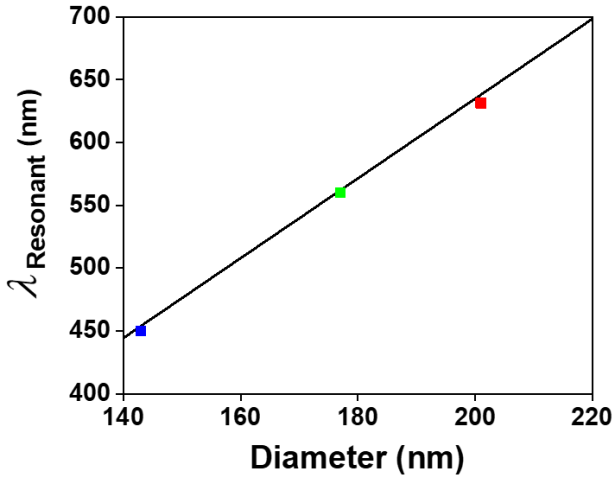

Figure S3. Resonant wavelength as a function of the diameter of silica particles. The solid line indicates the wavelength of Bragg's diffraction for (111) planes of nonclose-packed face-centered cubic (fcc) lattice.

S4. Nonclose-packed crystalline arrays

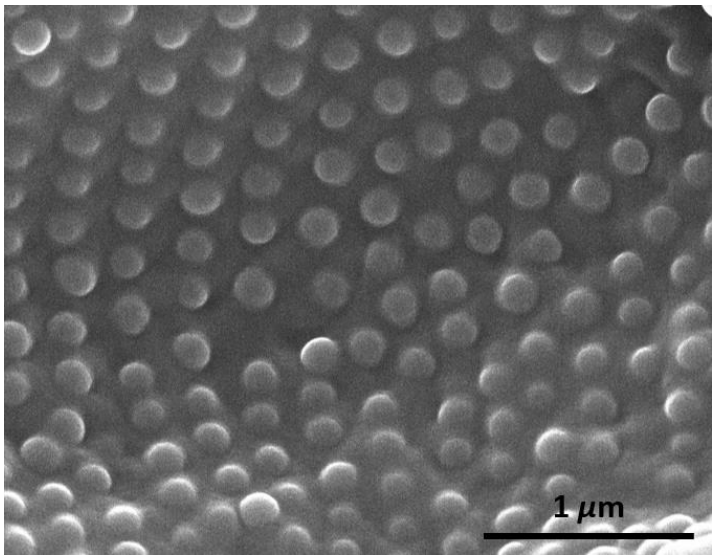

Figure S4. SEM image of the cross-section of photonic microbead, which shows nonclose-packed array of silica particles with a long-range crystalline order.

S5. Maximum diameter of polydopamine nanoparticles

In fcc lattice, there are two types of interstitial voids, one of which is octahedral and the other is tetrahedral, as shown in Figure S5. The maximum size of spherical particles that are accommodatable in the voids can be calculated by considering the geometry.

For the octahedral interstitial, the maximum diameter, d_m, of spherical particles is expressed as the difference between the lattice constant, a, and the diameter of particles, d, where the lattice constant is a function of d and ϕ:

$$d_m = a - d = \sqrt[3]{\frac{4\times\frac{\pi}{6}d^3}{\phi}} - d. \qquad (1)$$

With ϕ = 0.33, the values of d_m are 123 nm, 151 nm, and 171 nm for d = 143 nm, 177 nm, and 201 nm, respectively. For the tetrahedral interstitial, d_m is expressed as

$$d_m = 2\sqrt{3\times\left(\frac{a}{4}\right)^2} - d = 2\sqrt{3\times\left(\frac{1}{4}\sqrt[3]{\frac{4\times\frac{\pi}{6}d^3}{\phi}}\right)^2} - d. \qquad (2)$$

With ϕ = 0.33, the values of d_m are 87 nm, 107 nm, and 121 nm for d = 143 nm, 177 nm, and 201 nm, respectively.

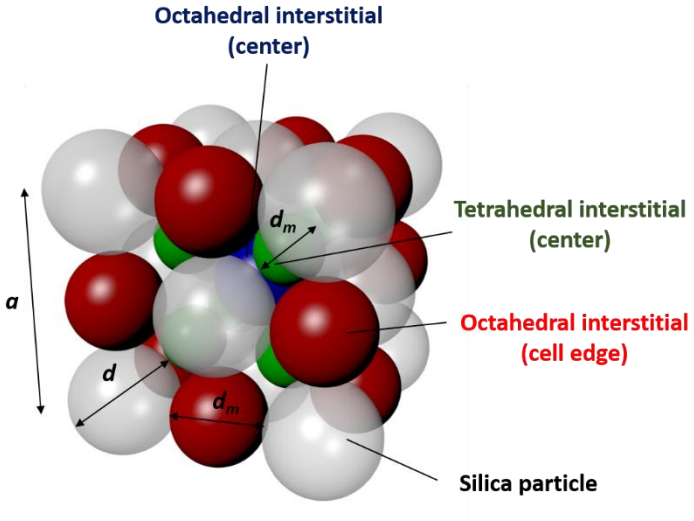

Figure S5. The unit cell of nonclose-packed fcc lattice, where octahedral interstitials are denoted with red and red spheres and tetrahedral interstitials are denoted with green spheres, respectively.

S6. Influence of polydopamine nanoparticles on optical appearance

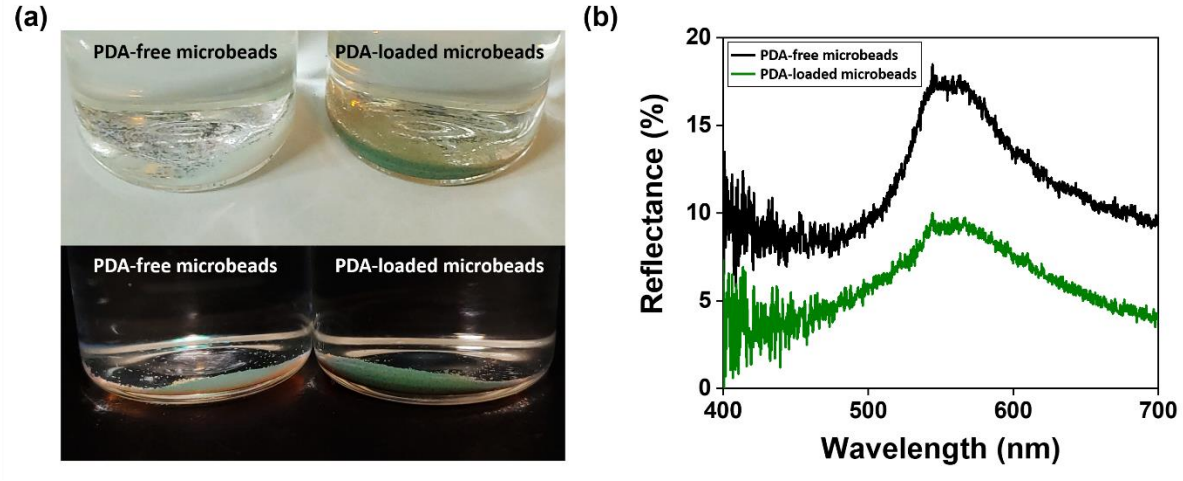

Figure S6. (a) Photographs of PDA-free microbeads (left) and PDA-loaded microbeads (right) on white (top) and black backgrounds (bottom). The PDA nanoparticles improve color saturation in both backgrounds. (b) Reflectance spectra of PDA-free microbeads and PDA-loaded microbeads.

S7. Microbead embedded in silicone matrix

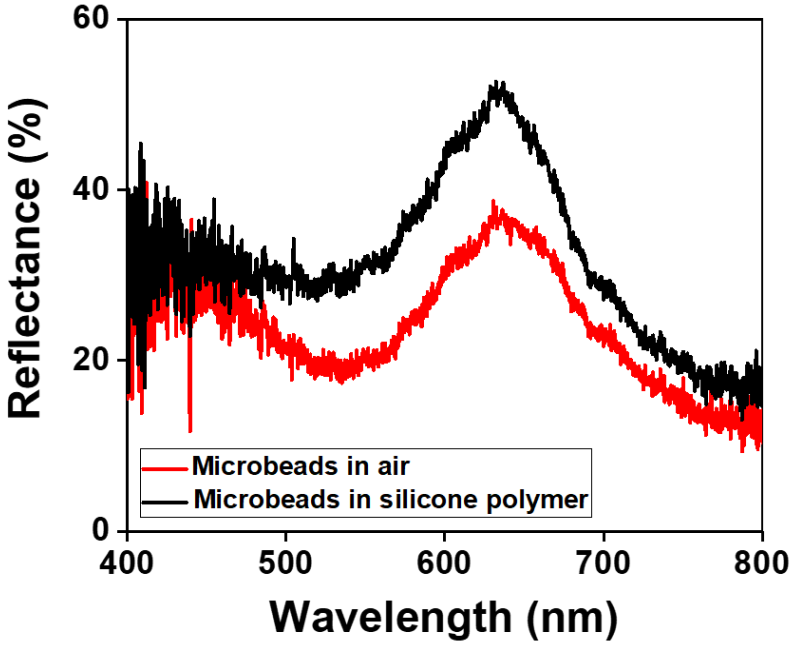

Figure S7. Reflectance spectra of microbeads exposed to air and embedded in silicone matrix.

S8. The optical property of microbead assembly

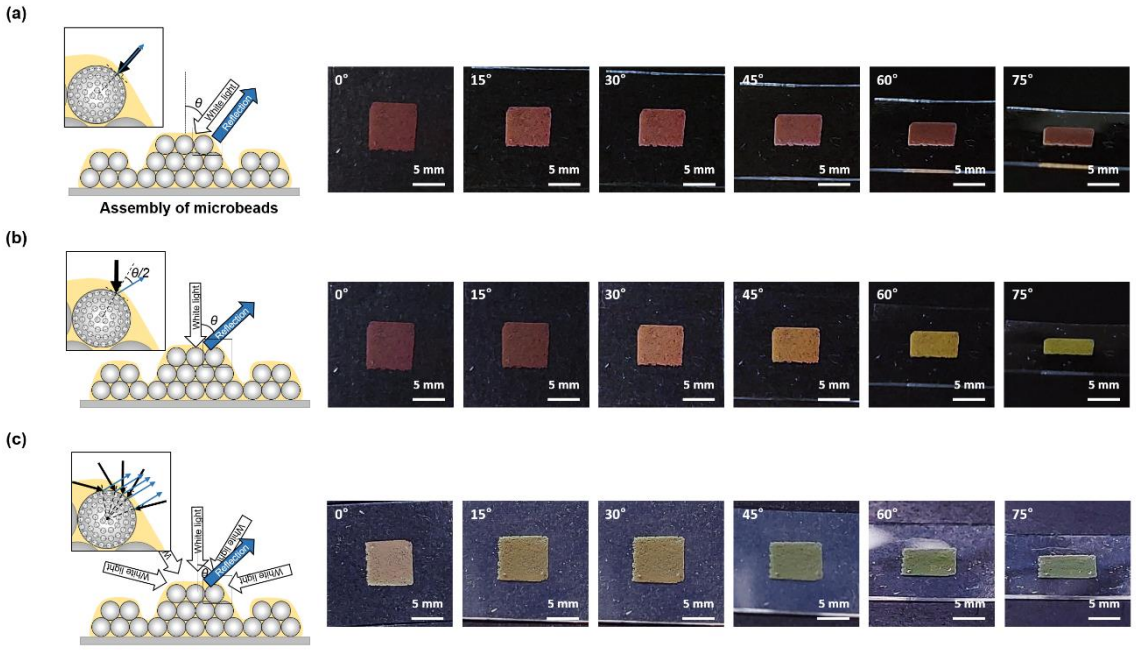

Figure S8. (a) Schematic illustration for imaging along the direction parallel to the unidirectional illumination (left) and a series of photographs of 2D film composed of red microbeads taken at various angles as denoted (right). The film shows no angle dependence. (b) Schematic illustration for imaging with various angles under unidirectional illumination normal to surface (left) and series of photographs (right). The film shows angle-dependent color change. (c) Schematic illustration for imaging with various angles under omnidirectional illumination (left) and series of photographs (right), where the photographs are taken outdoors. There is angle dependence.

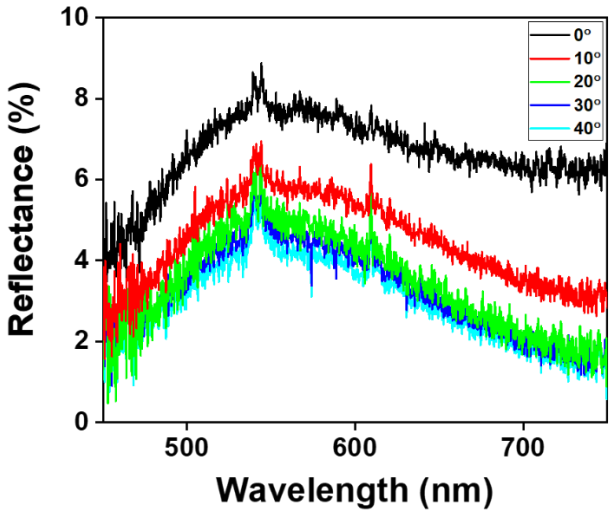

Figure S9. Series of reflectance spectra of K-pattern taken for the various angles of 0°, 10°, 20°, 30°, and 40°, where the unidirectional light is illuminated parallel to the measurement.

S9. The angle-dependent color change

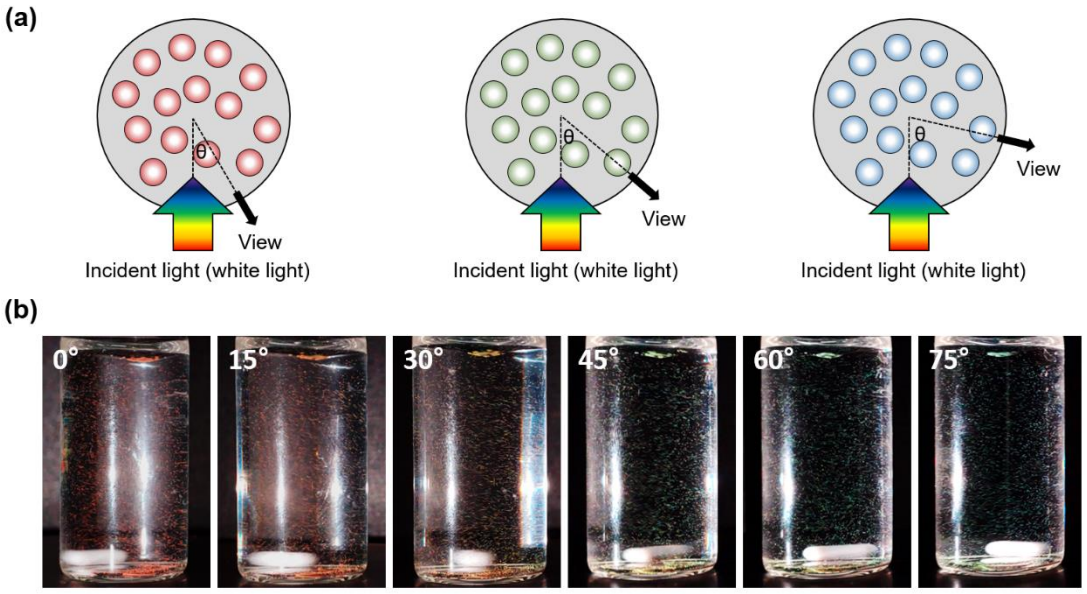

Figure S10. (a) Schematic illustration showing a set-up for imaging of a suspension of photonic microbeads. The incident beam is fixed while changing the angle of view, where θ denotes the angle between the incident beam and direction of observation. (b) A series of photographs showing the angle (θ)-dependent color change of a microbead suspension.

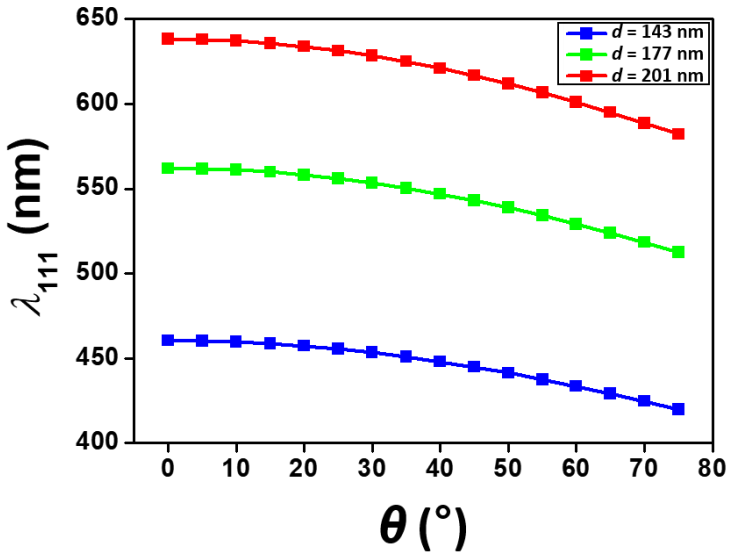

Figure S11. Variation of λ_{111} of photonic microbeads composed of silica particles with d = 143 nm (blue), 177 nm (green), and 201 nm (red) as a function of the angle, θ, between the incident light and observation direction for specular reflection, where the angle of reflection, φ, is set to $\theta/2$ in the eq. (1).

S10. Reflection of omnidirectional light on the surface of microbead

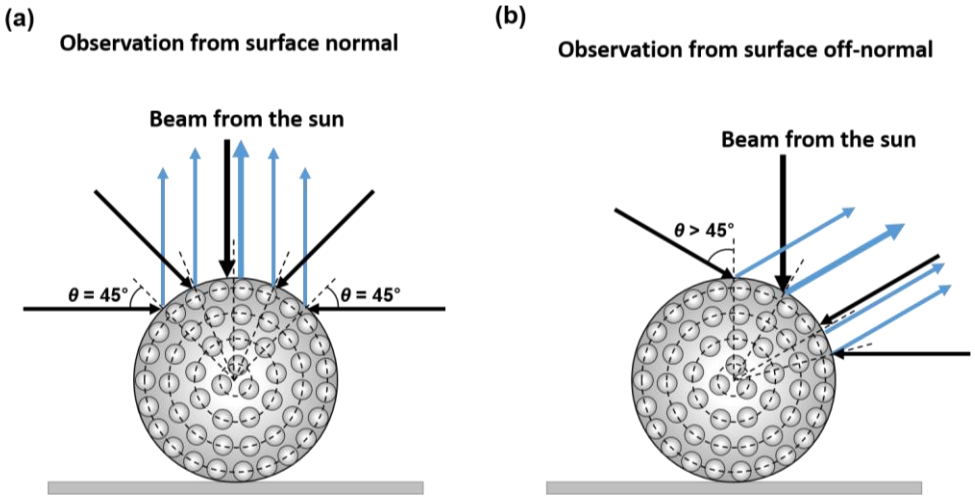

Figure S12. (a, b) Schematic illustrations showing the paths of beams reflected on the surface of microbead under omnidirectional illumination outdoor, where the direction of reflected beams is surface normal in (a) and off-normal in (b). A light directed from the sun is much stronger than others which is represented with a bold arrow. The reflection angle for the observation along surface normal is ranged from 0 to 45º, which makes a blue-shifted structural color for microbeads under omnidirectional illumination in comparison with those with unidirectional illumination with zero reflection angle. When the microbeads are observed surface off-normal under omnidirectional illumination, the range of reflection angle gets broader and the strongest beam from the sun also has a reflection angle, which makes additional blue-shift of structural colors along with the observation angle.

S11. Mechanical property

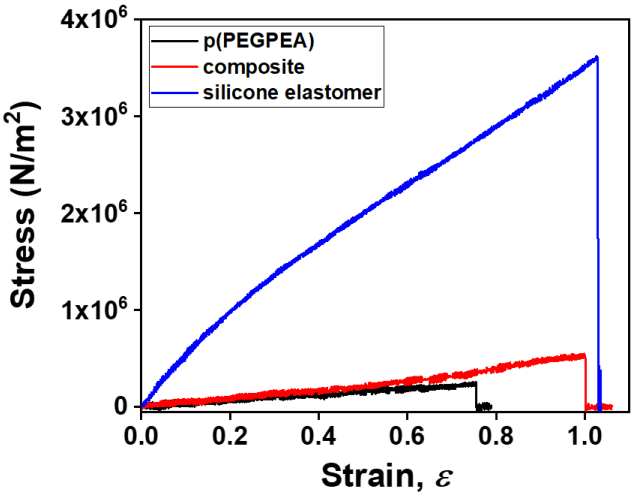

Figure S13. Stress-strain curves of particle-free pPEGPEA film (black), silica- and PDA-loaded photonic film (red), and silicone elastomer film used for the matrix of photonic microbeads (blue).

S12. Red-shift during compression of the microbead by Poisson effect

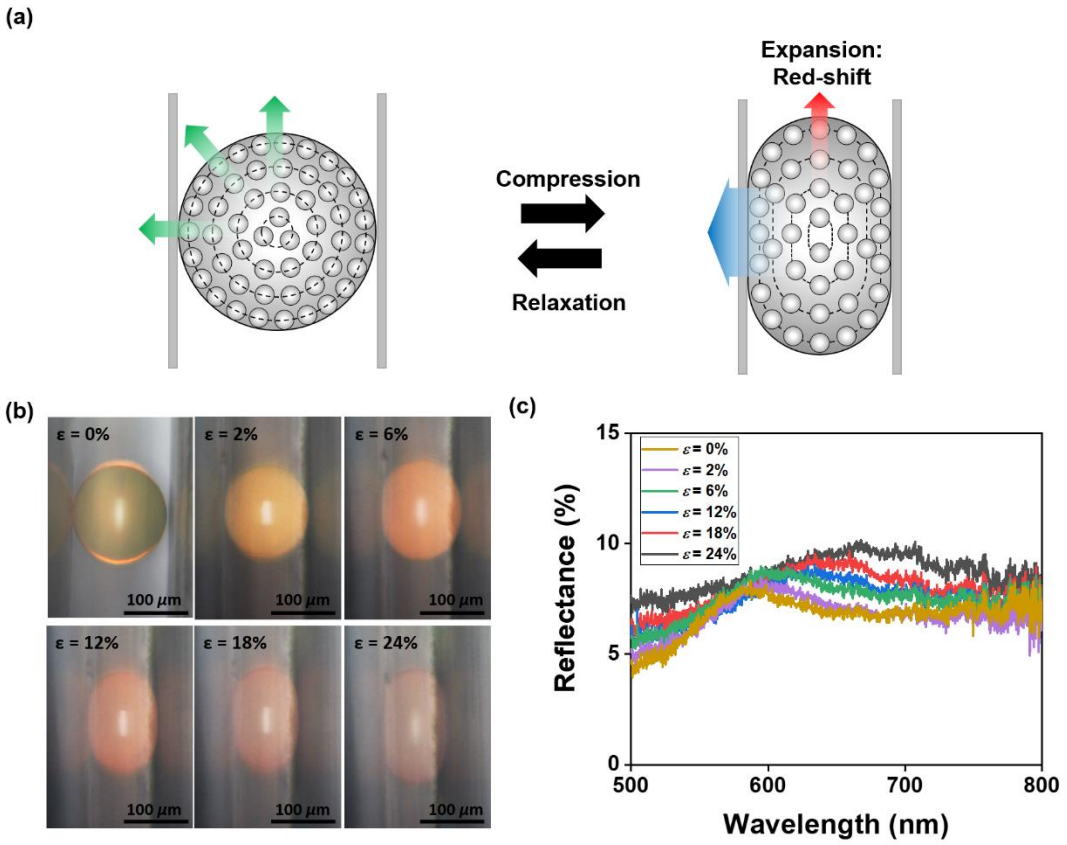

Figure S14. (a) Schematic illustration showing the deformation of the microbead by squeezed with a pair of plates, where the colloidal lattice is compressed along the direction of squeezing while expanded along the direction perpendicular to the squeezing due to Poisson effect. (b, c) A series of OM images (b) and reflectance spectra (c) of single microbead observed at the direction perpendicular to the squeezing. The color and reflectance peak red-shifts along with the compressive strain.

S13. Description for Supporting Movie

Movie S1

The movie shows stretching-induced color change and relaxation-induced color recovery of a 2D film composed of red microbeads embedded in a silicone elastomer matrix.